Phenanthrothiophene-Triazine Star-Shaped Discotic Liquid Crystals: Synthesis, Self-Assembly, and Stimuli-Responsive Fluorescence Properties

Chong-yang Zeng, Wen-jing Deng, Ke-qing Zhao, Carl Redshaw, Bertrand Donnio

▶ **To cite this version:**

Chong-yang Zeng, Wen-jing Deng, Ke-qing Zhao, Carl Redshaw, Bertrand Donnio. Phenanthrothiophene-Triazine Star-Shaped Discotic Liquid Crystals: Synthesis, Self-Assembly, and Stimuli-Responsive Fluorescence Properties. Chemistry - A European Journal, 2024, 10.1002/chem.202400296 . hal-04568178

HAL Id: hal-04568178
https://hal.science/hal-04568178

Submitted on 3 May 2024

HAL is a multi-disciplinary open access archive for the deposit and dissemination of scientific research documents, whether they are published or not. The documents may come from teaching and research institutions in France or abroad, or from public or private research centers.

L'archive ouverte pluridisciplinaire **HAL**, est destinée au dépôt et à la diffusion de documents scientifiques de niveau recherche, publiés ou non, émanant des établissements d'enseignement et de recherche français ou étrangers, des laboratoires publics ou privés.

Check for updates

Chemistry–A European Journal
Research Article
doi.org/10.1002/chem.202400296
Chemistry Europe
European Chemical Societies Publishing
www.chemeurj.org

Hot Paper

Phenanthrothiophene-Triazine Star-Shaped Discotic Liquid Crystals: Synthesis, Self-Assembly, and Stimuli-Responsive Fluorescence Properties

Chong-Yang Zeng,[a] Wen-Jing Deng,[a] Ke-Qing Zhao,*[a] Carl Redshaw,[b] and Bertrand Donnio*[c]

Lipophilic biphenylthiophene- and phenanthrothiophene-triazine compounds, **BPTT***n* and **CPTT***n*, respectively, were prepared by a tandem procedure involving successive Suzuki-Miyaura coupling and Scholl cyclodehydrogenation reactions. These compounds display photoluminescence in solution and in thin film state, solvatochromism with increasing solvent's polarity, as well as acidochromism and metal ion recognition stimuli-responsive fluorescence. Protonation of **BPTT**10 and **CPTT**10 by trifluoroacetic acid results in fluorescence quenching, which is reversibly restored once treated with triethylamine (ON-OFF switch). DFT computational studies show that intramolecular charge transfer (ICT) phenomena occurs for both molecules, and reveal that protonation enhances the electron-withdrawing ability of the triazine core and reduces the band gap. This acidochromic behavior was applied to a prototype fluorescent anti-counterfeiting device. They also specifically recognize Fe^{3+} through coordination, and the recognition mechanism is closely related to the photoinduced electron transfer between Fe^{3+} and **BPTT**10/**CPTT**10. **CPTT***n* self-assemble into columnar rectangular (Col_{rec}) mesophase, which can be modulated by oleic acid via the formation of a hydrogen-bonded supramolecular liquid crystal hexagonal Col_{hex} mesophase. Finally, **CPTT***n* also form organic gels in alkanes at low critical gel concentration (3.0 mg/mL). Therefore, these star-shaped triazine molecules possess many interesting features and thus hold great promises for information processing, liquid crystal semiconductors and organogelators.

Introduction

π-Conjugated star-shaped derivative molecules are renowned for their diverse photophysical and electronic properties, encompassing two-photon absorption, intramolecular charge transfer luminescence, stimuli-responsive luminescence, aggregation-induced luminescence, mesomorphism and high charge carrier mobility, properties that strongly depend on the core and attached arms.[1–8] In particular, trifold heteroatomic π-extended triazine derivatives exhibiting stimulated luminescence and semiconducting characteritics have been well documented for applications in organic light-emitting diodes, fluorescence sensing, biology cell imaging and solar cells.[9] Of particular interest, soft triazine-based smart materials endowed with stimuli-responsive luminescent ability, triggered by various external solicitations such as light, electric/magnetic field, heat, mechanic force, pH, solvent, etc. …, show promising application prospects in various domains such as optical anti-counterfeiting, fluorescence sensing, data processing and many other fields.[7–9] Owing to the N atoms present in the triazine structure, it is relatively easy to design multi-level stimuli-responsive systems, which can considerably broaden their scope of applications, e.g. through metal coordination, protonation, etc. … At present, while research on triazine derivatives has garnered considerable attention in the field of optics (i.e. two-photon absorption, single stimulus response, OLED, etc.), pharmaceutical and supramolecular materials,[7–9] there is a need to strengthen research on the performance of such multi-stimulus responsive luminescence materials. In addition, the optical and electronic behaviors of triazines are strongly contigent on their supramolecular arrangement and specific interactions with the local environment. Consequently, it is anticipated that their combination with the self-organization of liquid crystals holds significant potential.[1,8,10–13]

Discotic liquid crystals (DLCs) are particular attractive in this scientific research field in that they self-organize to form columnar nanostructures, which exhibit excellent defect self-reparation characteristics and potentially one-dimensional charge carrier transport capabilities.[14–18] When compared with

[a] C.-Y. Zeng, W.-J. Deng, Prof. K.-Q. Zhao
College of Chemistry and Materials Science
Sichuan Normal University
610066 Chengdu, China
E-mail: kqzhao@sicnu.edu.cn

[b] Prof. C. Redshaw
Department of Chemistry
University of Hull, School of Natural Sciences
Hull, HU6 7RX UK

[c] Dr. B. Donnio
Institut de Chimie et Physique des Matériaux de Strasbourg
UMR 7504, CNRS-University of Strasbourg
67034 Strasbourg, France
E-mail: bertrand.donnio@ipcms.unistra.fr

Supporting information for this article is available on the WWW under https://doi.org/10.1002/chem.202400296

© 2024 The Authors. Chemistry - A European Journal published by Wiley-VCH GmbH. This is an open access article under the terms of the Creative Commons Attribution License, which permits use, distribution and reproduction in any medium, provided the original work is properly cited.

© 2024 The Authors. Chemistry - A European Journal published by Wiley-VCH GmbH

traditional π-conjugated polymers and multi-domain crystalline materials, DLCs show usually higher charge carrier mobility and have several favorable characteristics that make them easier to process into thin film electronic devices by wet processing techniques.[14–18] Following the remarkable progress made in the last decade with the design of a great variety of luminescent molecular structures able to self-assemble into supramolecular columnar mesophases,[14] including polycatenar,[19] polyaromatic hydrocarbons (PAHs)[20] butterfly-[21] banana-,[22] and star-shaped,[1,6,8,22–29] liquid crystals, DLCs with a triazine core are able to combine various properties at once and permit to achieve multifunctional systems.[8,10–13] However, simple 1,3,5-triazine molecular systems decorated with lipophilic branches are not always conducive to columnar mesophases due to the free rotation of these groups around the σ bonds and the high conformational freedom of the molecules[10,11] Meanwhile, Yang *et al.*[30] reported that grafting π-conjugated triphenylene units to the triazine ring via short hydrazine-containing spacers, to yield dimers and trimers, was highly favorable to mesomorphism induction. Following this approach, Bai *et al.*[31] successively designed trimeric DLCs based on triazine and triphenylene species, linked through long flexible aliphatic spacers, all of them showing stable liquid crystal properties. In both cases, triphenylenes from neighboring trimers efficiently fill the space between the arms and limit free rotation concomittantly with the stabilization of the mesophases. With the presence of the lone electron-pair on the N atoms, the hydrogen-bonding stabilization strategy has also been reported.[7,32–34] This strategy consists in the insertion between the cavities of the triazine core of various hydrogen donating species to efficiently fill the space available. Such an elegant strategy opens up a new pathway for the construction of highly functional supramolecular DLC systems.

Another important ingredient in the construction of organic semiconductors is thiophene essentially due to the expansion of the S atomic orbitals, which can lead to more effective overlap of the π–π orbitals between molecules, enhancing intermolecular interactions[29,35] and improving charge carrier migration speed.[6,21,22,24] Early investigations have shown that the introduction of thiophene in π-extended aromatic systems is conducive to the formation of broad temperature-ranges columnar phases. In recent reports, it has also been found that thiophene-substituted triphenylene structures show remarkable liquid crystal behavior and present high charge carrier migration rates that can reach 10^{-3} $cm^2 \cdot V^{-1} \cdot s^{-1}$.[21] Last but not least, gel behavior has been observed in DLCs containing thiophene of importance for applications.[21,22] Both triazine and thiophene units can be employed to construct π-conjugated octupolar structures, which would be highly beneficial for both liquid crystal and stimuli-responsive performances in semiconducting materials.

Herein, we report the design and synthesis of **BPTT***n* and **CPTT***n* star-shaped compounds containing pendant discoid side-groups by a Suzuki-Miyaura coupling and Scholl oxidative cyclization tandem strategy.[36–39] Their liquid crystal behavior, gel properties and stimuli-responsive luminescence are studied in detail. Structure-property relationships are discussed, and the application of such systems in information storage explored.

Results and Discussion

Synthesis and Characterization

Based on various studies regarding the combination of stimulus-responsive fluorescence and liquid crystalline properties into one system, a series of new star molecules has been designed according to the following criteria: a large, planar π-conjugated aromatic core combining both electron-deficient and electron-rich units to construct intramolecular charge transfer (ICT) systems. We thus considered the electron-withdrawing triazine as the core of the molecule for which the lone-pair electrons on the N-atom will play a key role in building a stimulus-responsive molecule, i.e. that can be protonated by acid or coordinated to various metal ions, and on the other hand, the electron-rich tetraalkoxy phenanthro[9,10-*b*]thiophene (with long peripheral flexible chains $R = C_nH_{2n+1}$, $n = 10$, 12, and 14) as the branches to strengthen the intermolecular interactions to promote liquid crystal and organogelating properties (Scheme 1).

For the synthesis of these compounds, 2,4,6-tris(5-bromothiophen-2-yl)-1,3,5-triazine (**TT**) was synthesized by the trimerization reaction of 5-bromothiophene-2-carbonitrile catalyzed by trifluoromethanesulfonic acid (Scheme 1).[6] The star molecules **BPTT***n* ($n = 10/12/14$) were prepared by the Pd-catalyzed Suzuki-Miyaura cross-coupling of biphenyl borate ester[37,39] with the just mentioned bromothiophenetriazine (**TT**). **BPTT**10/12/14 were obtained with yields in the range of 72–87%, with the longer chain molecule affording the lowest yield due to its poorer solubility. Subsequently, the $FeCl_3$-catalyzed intramolecular Scholl cyclodehydrogenation resulted in the star-shaped phenanthro[9,10-*b*]thiophene derivatives **CPTT***n* ($n = 10/12/14$),

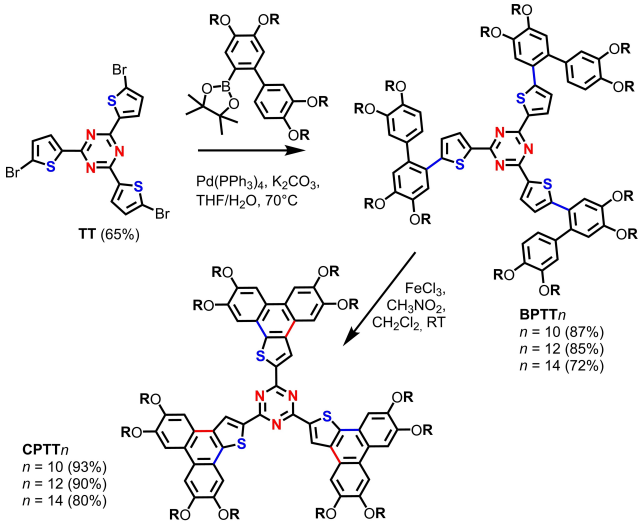

Scheme 1. Synthesis (Suzuki-Scholl tandem), nomenclature and yields of **BPTT***n* and **CPTT***n* compounds and precursor **TT** ($R = C_nH_{2n+1}$, with $n = 10$, 12, 14).

© 2024 The Authors. Chemistry - A European Journal published by Wiley-VCH GmbH

15213765, 0, Downloaded from https://chemistry-europe.onlinelibrary.wiley.com/doi/10.1002/chem.202400296 by Cochrane France, Wiley Online Library on [03/05/2024]. See the Terms and Conditions (https://onlinelibrary.wiley.com/terms-and-conditions) on Wiley Online Library for rules of use; OA articles are governed by the applicable Creative Commons License

with yields in the range of 80–90%, and again the longer chain exhibited the lowest yield due to the same solubility issue. The new star-shaped molecules were characterized by ^{1}H and ^{13}C NMR spectroscopy (Figure S1–S7), HRMS (Figure S8–S12) and EA. The experimental results were fully consistent with the proposed chemical structures.

Liquid Crystalline Behaviour

Before exploring the thermal behavior of the **CPTT***n* molecules, thermal gravimetry stability (TGA) was first carried out under N_2 atmosphere with a heating rate of 10 °C/min, and the results are shown in Figure S13 and Table S1. **CPTT***n* show good thermal stability, the initial thermal weight-loss temperatures are greater than 350 °C. The π-conjugated topology and the length of the flexible chains do not affect the thermal stability during the dynamic heating process ($T < 350$ °C).

The liquid crystalline properties of **BPTT***n* and **CPTT***n* were investigated by differential scanning calorimetry (DSC, Figure S14, Table S2) and polarizing optical microscope (POM, Figures 1a and S15a). As expected from its non-planar structure, LC mesophases were not observed in **BPTT***n* either on heating or cooling, while **CPTT***n* display wide mesomorphic temperature ranges on both heating and cooling (Figure 1b). Induction of mesomorphism thus is related to the increasing rigidity and flatness of the molecular structures. Optimization of the conformation of the model compounds by DFT calculations shows that **BPTT**1 exhibits a highly distorted conformation due to the large number of freely rotating σ bonds (Figure S16). On the contrary, **CPTT**1 has a nearly planar conformation i.e. propeller-like, and a highly π-extended conjugated aromatic core, which is conducive to more efficient and stronger π–π stacking interactions (also in agreement with the obvious change of the emission wavelength of the **CPTT**10 film as seen below in the study of photophysical properties). As the samples were slowly cooled from the isotropic liquid, **CPTT***n* display dendritic texture (Figure 1a), which is a typical texture of columnar mesophases. Due to the dipole interactions of N and S atoms and the strong π–π stacking between molecules, **CPTT***n* have also high clearing temperatures (Figure 1b), as high as 327 °C, and the mesophase ranges are as wide as 190 °C. The exothermic peak is shifted during the cooling process, which may be related to the high molecular weight and viscous melting state. Regardless of the heating or cooling process, all **CPPT***n* underwent a single-phase transition with a large enthalpy change ($\Delta H > 48.0$ kJ/mol) around 130 °C, corresponding to the mesophase-to-crystalline phase transitition as confirmed by POM. In addition, the clearing temperatures decrease and the mesophase ranges narrow with increasing alkoxy chain length, mainly due to the entanglement of the alkoxy chains affecting the effective stacking between molecules.

The mesophases of **CPTT***n* were further characterized by small- and wide-angle X-ray scattering (S/WAXS), and their self-assembly modes within the mesophases explored (Figures 2a and S18–19, Table S3). In all cases, the S/WAXS patterns were

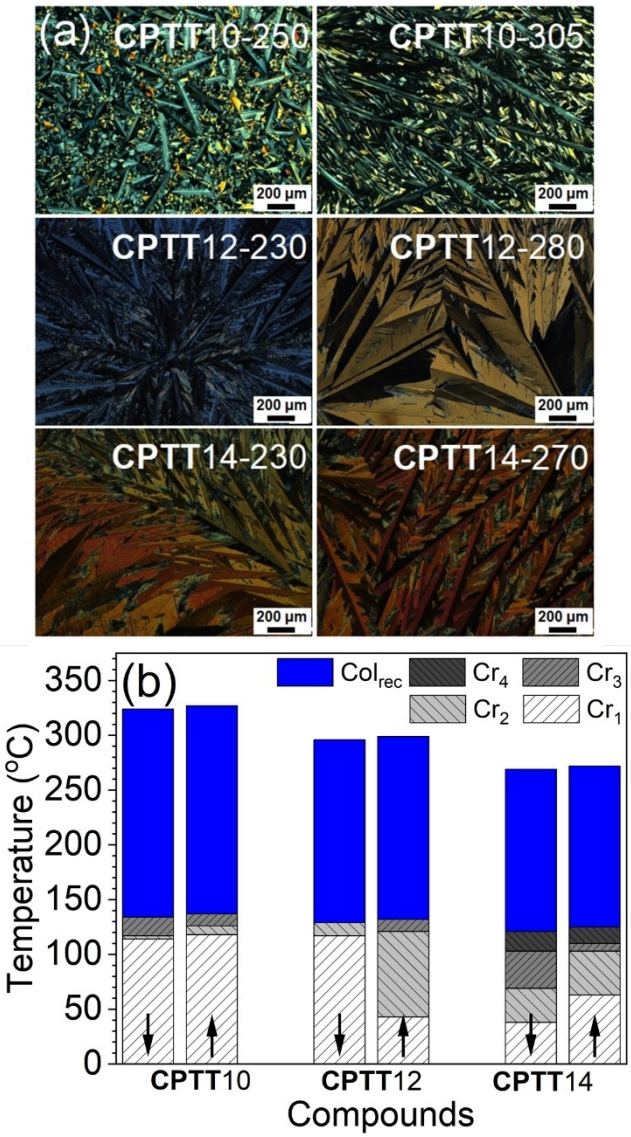

Figure 1. (a) POM photomicrographs of **CPTT***n* at various temperatures on cooling from the isotropic liquid; (b) Phase diagram of **CPTT***n* on heating and cooling (black arrows); Cr_i: crystalline phases.

rather simple, suggesting the formation of single molecular columns ($Z_{col} = N_{mol}$) unlike our previously reported triazine system.[8a] They exhibit systematically only two intense and sharp diffraction peaks in the small angle region resulting from the self-assembling of the star-shaped compounds into columns, which are located at the nodes of the 2D ordered rectangular lattices ($Z_{col} = 2$), and two (or three) additional broad scattering signals in the wide-angle region corresponding respectively to the molten alkoxy chains dispersion ($h_{ch} \approx 4.0$–4.5 Å, weak π–π stacking ($h_{\pi} \approx 3.6$–3.8 Å) and to some short-range intermolecular interactions ($h_{mol} \approx 7.0$–7.4 Å), which could a priori correspond to the average distance between successive triazine cores piled in columns (See Figure 2b). The increase of peripheral flexible chains or the decrease of temperature (in the range of mesophase) contribute to the increase of lattice the parameters of **CPTT***n*.

© 2024 The Authors. Chemistry - A European Journal published by Wiley-VCH GmbH

15213765, 0, Downloaded from https://chemistry-europe.onlinelibrary.wiley.com/doi/10.1002/chem.202400296 by Cochrane France, Wiley Online Library on [03/05/2024]. See the Terms and Conditions (https://onlinelibrary.wiley.com/terms-and-conditions) on Wiley Online Library for rules of use; OA articles are governed by the applicable Creative Commons License

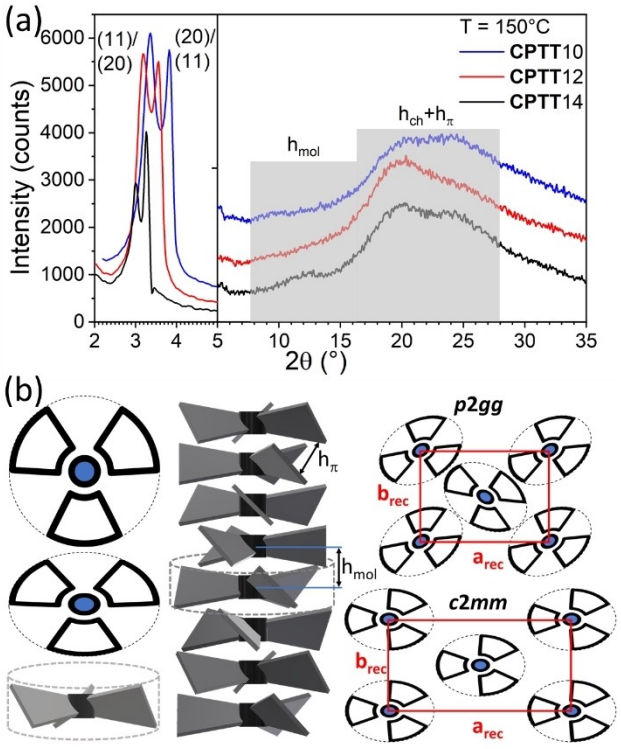

Figure 2. a) Small- and wide-angle X-ray scattering (S/WAXS) patterns of the Col_{rec} mesophase of **CPTT***n* compounds recorded on cooling at 150 °C. b) Schematic representation of the 3-bladed propeller molecules (top and side-views), and projections on lattice plane without (circular) and with (elliptical) molecular tilt, and side-view of the columns made of stacked molecules with random orientational changes (molecular tilt not represented); molecular slice thickness h_{mol} compared to π-stacking distance, h_{π}; the two solutions are shown, and drawn at the same scale, with elliptical columns arranging in rectangular lattices with parameters a_{rec} and b_{rec}; the ellipses adopt alternated orientations with respect to a-axis (*p2gg*) or are collinear to a-axis (*c2mm*); aliphatic chains are not shown for clarity.

With only two fundamental reflections, the indexation is however not unequivocal, and both possible indexing solutions, corresponding to the two highest rectangular symmetries (*p2gg* and *c2mm*), have been considered (Table S3) i.e. both signals corresponding to the lowest and highest angle reflections can be assigned as 11 and 20, or vice et versa, respectively. Note that for the longest chain homolog, **CPTT**14, another weak reflection could be found, and indexed as either 12 or 31, depending on the indexing solution considered (Table 1), but which unfortunately was not sufficient to lift the degeneracy. The first possibility thus gives a rectangular lattice with a *p2gg* symmetry (due to reflection 12), and a parameters ratio a/b almost equal to 1.5, whereas for the other possibility, the lattice of highest symmetry, *c2mm*, was considered, and the ratio increases to nearly 2 (Table 1). None of these two solutions can yet be excluded. As shown by DFT (Figure S16), due to both the free rotation between the triazine center and the three pending mesogenic groups around the σ-bonds, and to the steric effect of the numerous aliphatic side-chains, the star-shaped molecules cannot expand in the same plane and have to diverge from it to take on likely the shape of a three-bladed propeller with the out-of-plane deviation of the pending disc-like mesogenic units (Figure 2b). Depending on the torsion angle between the triazine and the mesogenic groups, which is not known, the molecular thickness or average distance between two successive molecules is necessarily larger than the expected π–π stacking. Furthermore, the rectangular symmetry of the mesophases implies that the columns possess an elliptical cross-section, which requires an additional inclination of the molecules with respect to the lattice plane.

The values of the molecular slices' thicknesses or molecular seperation, h_{mol}, can be simply deduced from the ratio between the molecular volume and the columnar area, according to $h_{mol} = N_{mol} \times V_{mol}/A$ and for $N_{mol} = 2$, are about 6.4–6.5 and 7.5 Å for the *p2gg* lattice, and around 7.0–8.0 Å for the *c2mm* lattice, at both low and high temperature, respectively, in good agreement with the experimental measurements (Table S3). Thus, the propeller molecules stack into single column, and each column is surrounded by 12 chains and arranged in one or the other rectangular cell.

The triazine core is also an outstanding block for the construction of hydrogen-bonding supramolecular columnar mesophases.[40] Indeed, the void left between the arms can be efficient filled by small hydrogen-donating molecules, which in turn can modify the mesomorphic properties.[7,32–34] In the following acidochromic study, **CPTT**10 proved capable of recognizing an acid proton and was therefore used to construct hydrogen-bonded supramolecular liquid crystals in an attempt to modulate the mesomorphic behavior. Hexanoic acid was first utilized to form a complex with **CPTT**10. Examination of POM texture, clearing temperature and mesophase range did not reveal any significant changes from the pure compound, which could be due to the low boiling temperature of hexanoic acid leading to fast thermal decomposition of the supramolecules and to restoring of pure **CPTT**10. Higher-boiling temperature oleic acid (OA) was subsequently selected to react with **CPTT**10. Both species were mixed in dichloromethane in the 3:1 molar ratio, stirred for 4 h, and dried to yield the supramolecular hydrogen-bonded complex **CPTT**10-OA (Figure 3a). The formation of a 3:1 supramolecular compound was inferred by ^{1}H NMR and IR spectroscopies. The low field shift of the proton signals in ^{1}H NMR spectrum proves the formation of H-bonds (Figure 3b). The new IR absorption at 3442 cm^{-1} in the infrared spectrum of **CPTT**10-OA was attributed to the N–H stretching vibration, and the stretching vibration peak of the carbonyl group appeared near 1710 cm^{-1}, which is also consistent with the formation of a H-bonded supramolecular compound (Figure 3c). These observations were consistent with other recently reported hydrogen-bonded supramolecular compounds of triazine.[7,32–34] Further, the mesomorphism of **CPTT**10-OA was also studied by POM, DSC and S/WAXS. A distinct fan-shaped focal conical texture from neat **CPTT***n* was observed by POM, along with the presence of large homeotropic domains, typical of hexagonal columnar mesophase (Figure S15b). The clearing temperature was reduced down by 142 °C, significantly lower than that of pure **CPTT**10, and the mesophase range was consequently much reduced (Figure S14). The long alkyl chain of the oleic acid plays a space filling role, as well as dilutes the aromatic core and π–π interactions, which can explain the huge

© 2024 The Authors. Chemistry - A European Journal published by Wiley-VCH GmbH

15213765, 0, Downloaded from https://chemistry-europe.onlinelibrary.wiley.com/doi/10.1002/chem.202400296 by Cochrane France, Wiley Online Library on [03/05/2024]. See the Terms and Conditions (https://onlinelibrary.wiley.com/terms-and-conditions) on Wiley Online Library for rules of use; OA articles are governed by the applicable Creative Commons License

Table 1. Mesophases' geometrical parameters.

Compound/ Mesophase	Temperature[a]	V_{mol}, ρ[b]	Solution 1 a, b[c]	A, R[c]	N_{mol}, h_{mol}[d]	Solution 2 a, b[c]	A, R[c]	N_{mol}, h_{mol}[d]
CPTT10	150	4720 (0.934)	46.34 32.05	1485.2 1.44	2 6.36	52.72 25.79	1359.6 2.04	2 6.94
Col_{rec}	270	5260 (0.824)	44.92 31.28	1405.1 1.44	2 7.49	51.34 24.98	1282.5 2.05	2 8.20
CPTT10-OA Col_{hex}	140	6340 (0.928)	30.58	810	1 7.83	–	–	–
CPTT12	150	5430 (0.914)	50.02 33.40	1670.7 1.50	2 6.50	55.56 28.01	1556.2 1.98	2 6.98
Col_{rec}	270	6030 (0.824)	49.08 32.96	1617.7 1.49	2 7.46	54.72 27.46	1502.6 1.99	2 8.03
CPTT14	150	6140 (0.900)	53.7 35.25	1893.1 1.52	2 6.49	58.94 30.16	1777.7 1.95	2 6.91
Col_{rec}	240	6620 (0.835)	51.6 34.36	1773.0 1.50	2 7.47	57.2 28.91	1653.6 1.98	2 8.00

[a] Temperature of experiment (°C); [b] Molecular volume (Å^3) and density (g cm^{-3}) calculated from partial volumes of reference substances: $V_{mol} = V_{ar} + V_{ch}$, the sum of the volume of the aromatic part, V_{ar} (from reference compounds) and the volume of the chains, V_{ch};[41] $\rho = MW/(N_A.V_{mol})$; [c] Lattice parameters, a and b (Å) and area, $A = a \times b = a_{rec} \times b_{rec}$ for Col_{rec} and $A = a^2\sqrt{3}/2$ ($a = a_{hex}$) for Col_{hex}; R, aspect ratio, $R = a_{rec}/b_{rec}$; [e] N_{mol}, number of molecules per lattice, and h_{mol}, molecular thickness, $h_{mol} = N_{mol} \times V_{mol}/A$.

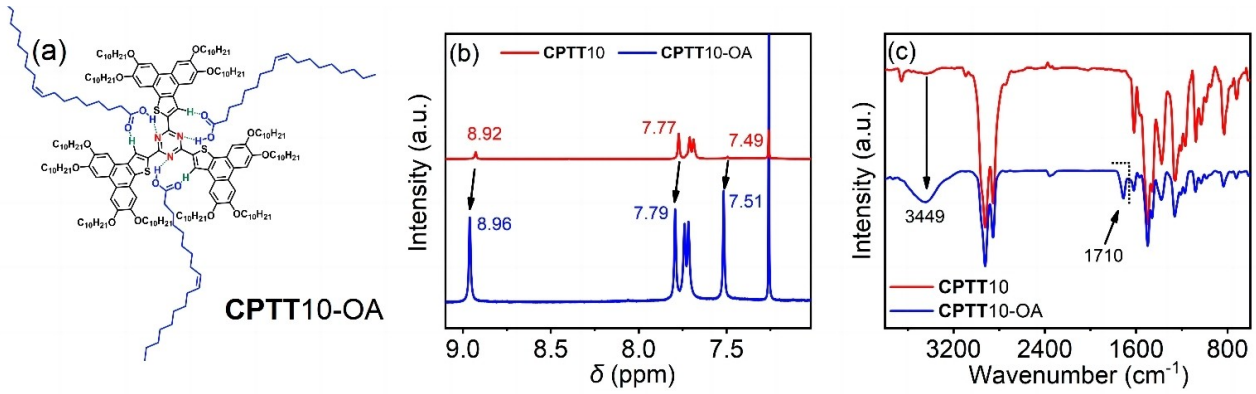

Figure 3. (a) Molecular structure of the H-bonding supramolecular complex **CPTT**10-OA; (b) ^{1}H NMR ($CDCl_3$) and (c) infrared spectra of **CPTT**10 and **CPTT**10-OA.

fall of the clearing temperature. The thermal stability of the hydrogen bonding complex was confirmed by repeating POM experiments on slow cooling from the isotropic liquid (Figure S15b) with no signs of decomposition and/or phase separation detected. The S/WAXS pattern recorded at 140 °C on cooling from the isotropic liquid (Figure S19) revealed the presence of only one single and intense reflection in the small angle range ($2\theta = 3.333°$, $d_{10} = 26.48$ Å) along the broad scattering in the wide-angle part ($2\theta = 24.79°$, $h_{ch} = 3.59$ Å) corresponding to the molten chains. The presence of only one reflection agrees with the formation of a Col_{hex} phase, confirming the POM observations. As the mesophase symmetry is increased to hexagonal, the columns have a circular cross-section, and the calculated value of the molecular slice' thickness, h_{mol}, is about 7.83 Å i.e. slightly more stretched than for the pure compound, and it confirms the inclusion of the oleic acid space filler.

Gelling Behaviour

Polycyclic aromatic hydrocarbons (PAH) decorated with long alkyl chains usually form gels in various organic solvents.[42] Organic gels are widely studied in biomedicine and pharmaceuticals. The formation of gels is due to intermolecular interactions (such as π–π stacking, dipole interaction, hydrogen bonding, etc.) that allow molecules to self-assemble into supramolecular structures in solvents, locking solvent molecules in intermolecular voids. Gel behavior has been found in H-bonded[42] and extended fluorine triphenylene π-systems,[43] whereas it is commonly observed in liquid crystalline polymers.[42,44] Given this, the self-assembly of **CPTT***n* and **BPTT***n* into gels in different solvents was explored. When temperature decreases or concentration increases, **CPTT***n* can easily form a gel in an organic solvent and exhibit a sol/gel transition. Unfortunately, this gel behavior was not present for **BPTT***n*

© 2024 The Authors. Chemistry - A European Journal published by Wiley-VCH GmbH

15213765, 0, Downloaded from https://chemistry-europe.onlinelibrary.wiley.com/doi/10.1002/chem.202400296 by Cochrane France, Wiley Online Library on [03/05/2024]. See the Terms and Conditions (https://onlinelibrary.wiley.com/terms-and-conditions) on Wiley Online Library for rules of use; OA articles are governed by the applicable Creative Commons License

compounds even when the concentration reached 20 mg/mL. Gel formation is thus likely due to the more rigid and more planar core of **CPTT***n* than **BPTT***n* (DFT), and thus to more efficient π–π intermolecular interactions between the tetraalkoxy phenanthro[9,10-*b*]thiophene units.

The concentration-dependent ^{1}H NMR spectroscopic experiments (Figure S20) show that on increasing the concentration, the aromatic hydrogens (Ar**H**) undergo a significant high-field shift. This is the result of molecular aggregation leading to an increase in the change of π–π interaction surface-to-surface proximity and the shielding of aromatic hydrogen atoms by the aromatic electron flux. Among them, the shift of $\mathbf{H}_t$ on the thiophene is the most obvious (7.64 ppm→7.49 ppm) compared to the change of Ar**H** on the biphenyl (such as $\mathbf{H}_p$, 7.89 ppm→7.77 ppm). This also shows that thiophene is essential to enhance intermolecular interactions. Then, **CPTT**10, as a representative example was selected to explore gel properties in various common solvents and to measure critical gel concentration (CGC) for its gel ability (Figure 4). The mixtures were completely dissolved by heating and then cooled down to room temperature. In both polar and non-polar solvents, **CPTT**10 can form room temperature transparent gels, which exhibit the same fluorescence as the film under a UV lamp. **CPTT**10 has the lowest CGC value of 3.0 mg/mL in hexane and cyclohexane. Early reports[42] have shown that the growth of flexible chains contribute to the formation of gels. Therefore, we speculate that **CPTT**12 and **CPTT**14 will have an even lower critical gel concentration. In order to further analyze the gel behavior, xerogels from the different organic solutions were prepared by the freeze-drying method, and characterized by scanning electron microscopy (SEM, Figures 4 and S21–S25). The gel morphology of **CPTT**10 shows an obvious solvent dependence, forming linear (Figure 4a), lamellar (Figure 4b), thin plate (Figure 4d) and three-dimensional (3D) grid (Figure 4c, e) morphologies in different solvents. Therefore, **CPTT***n* has good gel behavior and has potential application value in the field of organic gels.

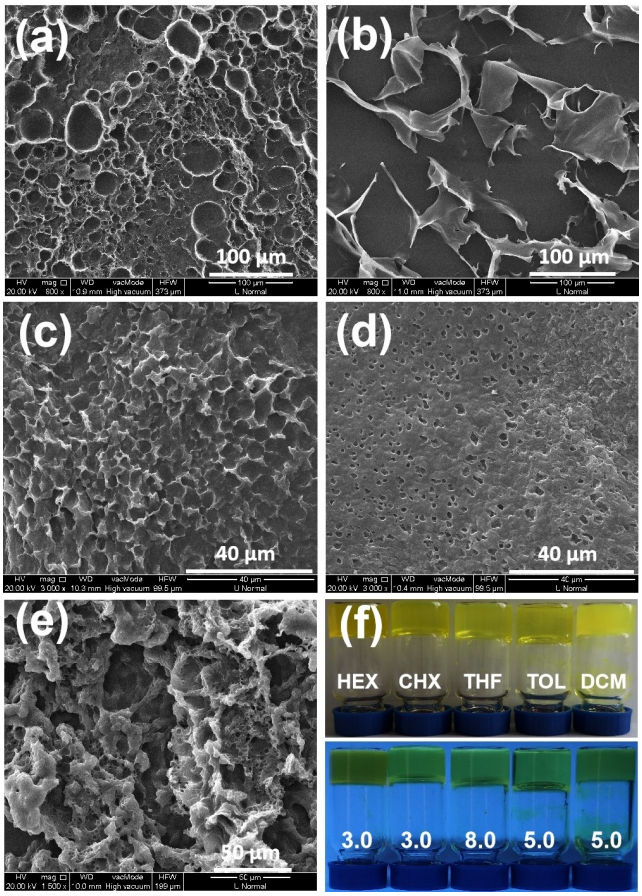

Figure 4. Scanning electron microscopy (SEM) images of **CPTT**10 self-assembled gels in hexane – HEX – (a), cyclohexane – CHX – (b), tetrahydrofuran – THF – (c), toluene – TOL – (d) and dichloromethane – DCM – (e) after freeze-drying; (f) Inverted tube photo of the organic gel formed by **CPTT**10 in solvent under sunlight (up) and a UV lamp (bottom), the number on the glass tube indicates the critical gel concentration (CGC, mg/mL) of the gel formed in the solvent. Additional SEM images can be seen in the supplementary information (Figures S21–S25).

Photophysical Properties and Solvatochromism

The photophysical properties of **BPTT***n* and **CPTT***n* were studied by measuring their UV-Vis absorption and fluorescent spectra in THF (Figures 5a and S26). Increasing the alkyl chain length did not change the photophysical properties much. Thus, the subsequent optical properties study were focused on **BPTT**10 and **CPTT**10 as representative examples. In THF, **BPTT**10 possesses three absorption bands of different intensities located at 290, 310 and 405 nm respectively, whilst **CPPT**10 has only two absorption bands at 290 and 430 nm. The molar extinction coefficients (*k*) of all absorption bands were greater than 10^4 L·mol^{-1}·cm^{-1}. DFT optimized molecular conformation calculations (Figure S16) of model compounds **BPTT**1 and **CPTT**1 (*i.e.* the long alkyl chains R are replaced by -Me for simplifying the calculations) show that **BPTT**1 is not planar and exhibits less π-conjugation than, in contrast, to **CPTT**1, which is almost

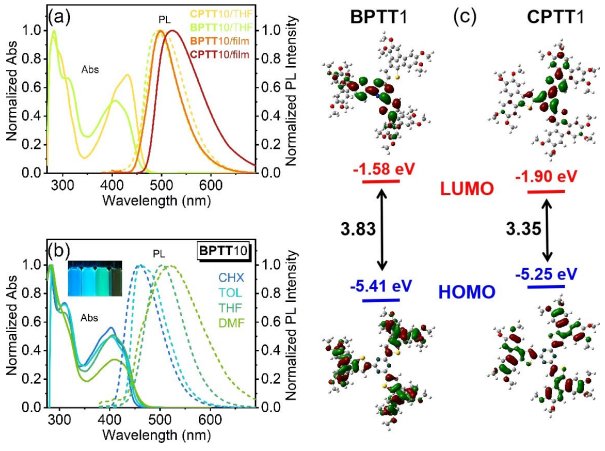

Figure 5. Photophysical properties of the thiophene-triazine compounds. (a): UV-Vis. absorption and photoluminescence spectra of **BPTT**10 and **CPTT**10 in THF and thin film; (b): UV-Vis. absorption and photoluminescence spectra of **BPTT**10 in different polar solvents (insert shows fluorescence photos of **BPTT**10 in different solvents, the polarity increasing from left to right); (c): HOMO-LUMO and band gap of **BPTT**1 and **CPTT**1.

© 2024 The Authors. Chemistry - A European Journal published by Wiley-VCH GmbH

15213765, 0, Downloaded from https://chemistry-europe.onlinelibrary.wiley.com/doi/10.1002/chem.202400296 by Cochrane France, Wiley Online Library on [03/05/2024]. See the Terms and Conditions (https://onlinelibrary.wiley.com/terms-and-conditions) on Wiley Online Library for rules of use; OA articles are governed by the applicable Creative Commons License

planar after thiophene annulation. This results in the absorption of **CPTT**10 being both red-shifted and broader. The fluorescence spectra show that **BPTT**10 (Figure 5b) and **CPTT**10 (Figure S26) exhibit photoluminescence in both THF and as films, with absolute quantum yields (QY) of 59% for **BPTT**10 and of only 12% for **CPTT**10 (Table 2). The frontier molecular orbitals (FMO) of **BPTT**1 and **CPTT**1 obtained by DFT (Figure 5c) calculations show that their HOMO electrons are distributed on the biphenyl and thiophene moieties, whilst the LUMO electrons are focused on the central triazine core, *i.e.*, in agreement with intramolecular charge transfer (ICT) between the central core toward the peripheral groups. In addition, the HOMO-LUMO gap of **CPTT**1 (3.35 eV) is substantially narrower than that of **BPTT**1 (3.83 eV), due to the extended π-conjugation, which resulted in a red-shift of the absorption and emission spectra. The annulated, extended π-system of **CPTT**10 thus facilitates the formation of ordered aggregates at the origin of the appearance of a liquid crystal phase and organic solvent gelation (see above). These strong interactions between side-arms and with solvent molecules concomitantly contribute to the increase of non-radiative decay and weakening of the fluorescence, and thus to the lowering of the emission QY of **CPTT**10 i.e. aggregation-caused quenching, ACQ, effect as compared to **BPTT**10.

The solvatochromism of the absorption and emission for **BPTT**10 and **CPTT**10 was examined in two nonpolar solvents, namely cyclohexane (CHX) and toluene (TOL), and two polar solvents, namely DMF and THF (Figures 5b and S27, Tables 2 and S4). As the solvent polarity increases, the vibration and rotation of the molecule are limited, resulting in the disappearance of the fine structure in the UV absorption spectra, the decrease of the molar extinction coefficient and the red shift of the emission maxima. The emission of **BPTT**10 was red shifted by 67 nm, and that of **CPTT**10 by only 23 nm, whilst the emission was weakened for both. We speculate that **CPTT**10 is prone to self-assembly into aggregates in cyclohexane, resulting in aggregation-caused quenching and a reduced fluorescence quantum yield (the aggregation phenomenon discussed in the gel section above, and the aggregation-caused quenching phenomenon can be confirmed by the emission spectra, Figure S28, of **CPTT**10 in THF/H_2O mixed solvents with different water fractions). Meanwhile, in DMF the quantum yield could hardly be detected because of the decrease of the number of luminescent molecules due to solubility issues. The correlation between the directional polarizability (Δf) and the Stokes shift (Δv) of **BPTT**10 and **CPTT**10 was fitted by the Lippert-Magata equation (Table S4 for details). It was found that the fit line was good (Figure S29), which proves that the polarity of the ground state is smaller than that of the excited state during the transition. The Lippert-Magata equation estimates that the dipole moment changes between the excited state and the ground state during the transition of **BPTT**10 and **CPTT**10 by 16.25 D and 10.24 D, respectively. In polar solvents, the stability of the solvent to the excited state is enhanced, and the energy difference of the π–π* transition reduced, resulting in the red shift. It is worth mentioning that the slope of **BPTT**10 (9269) is 5.2 times steeper than that of **CPTT**10 (1794), consistent with a greater polarity in the excited state for **BPTT**10. Furthermore, the twisted structure might be accompanied by the twisted intramolecular charge transfer (TICT) state in the highly polar solvent resulting in a decrease in the fluorescence.[39] **BPTT**10 is more sensitive to solvent polarity than **CPTT**10, and a good linear relationship obtained by Lippert-Magata fitting ($R^2 = 0.99$) suggests that **BPTT**10 has the potential as a solvent polarity probe. The fitting results of the ET(30) equation, which is another method related to the Stokes shift and solvent polarity, also show the same correlation (Figure S29), *i.e.*, the slope of the fitting line of **BPTT**10 is 5 times that of **CPTT**10. In summary, both **BPTT**10 and **CPTT**10 exhibit solvatochromism, which provides a way for visual recognition of solvents and has the potential to develop lyotropic fluorescent probes.

Table 2. Photophysical properties and related solvent parameters of triazine **BPTT**10 and **CPTT**10.

Compds	Solvent	λ_{ab}[a]	k ($\times 10^4$)[b]	λ_{em}[c]	QY[d]	$\Delta\nu$[e]
BPTT10	CHX	402	7.3	455	68	2898
	TOL	405	7.2	461	65	2999
	THF	406	6.6	498	59	4550
	DMF	409	7.0	522	32	5292
CPTT10	CHX	429	4.6	473	7	2168
	TOL	429	2.7	490	13	2901
	THF	430	2.6	500	12	3255
	DMF	432	0.1	492	–	2823

Photophysical parameters: [a] λ_{ab}: UV absorption wavelength (nm); [b] *k:* molar extinction coefficient ($L \cdot mol^{-1} \cdot cm^{-1}$); [c] λ_{em}: emission wavelength (nm); [d] QY: quantum yield (%); [e] Δv: Stokes shift, $\Delta v = \lambda_{ab} - \lambda_{em}$ (cm^{-1}).

Acidochromism

Acidochromic materials have been widely used in acid-base indication and information processing in recent years.[8] Therefore, it is valuable to develop novel and more sophisticated acid-base stimuli color-change materials. As triazine is an easily protonated aromatic block, the acidochromism of **BPTT**10 and **CPTT**10 was studied, and the results are summarized in Figures 6 and S30. When trifluoroacetic acid (TFA) was successively added to the chloroform solution of **BPTT**10, the absorption peak at 395 nm gradually weakened and a new peak at 505 nm appeared (Figure 6a). Its absorption was red-shifted by 110 nm and the fluorescence intensity gradually weakened until quenched (Figure 6b). The same phenomenon was observed for **CPTT**10 when it was treated by TFA (Figure S30). The fluorescence quenching and absorption red-shift indicate that new complexes had formed for **BPTT**10 and **CPTT**10 with TFA. The absorption and fluorescence were reproduced in a reversible manner when the acidified solution was treated with triethylamine (TEA). When the solutions were treated alternately with TFA and TEA, the fluorescence emissions could be switched between 'off and on' states multiple times (Figure 6c). The molecular structures of **BPTT**10

© 2024 The Authors. Chemistry - A European Journal published by Wiley-VCH GmbH

15213765, 0, Downloaded from https://chemistry-europe.onlinelibrary.wiley.com/doi/10.1002/chem.202400296 by Cochrane France, Wiley Online Library on [03/05/2024]. See the Terms and Conditions (https://onlinelibrary.wiley.com/terms-and-conditions) on Wiley Online Library for rules of use; OA articles are governed by the applicable Creative Commons License

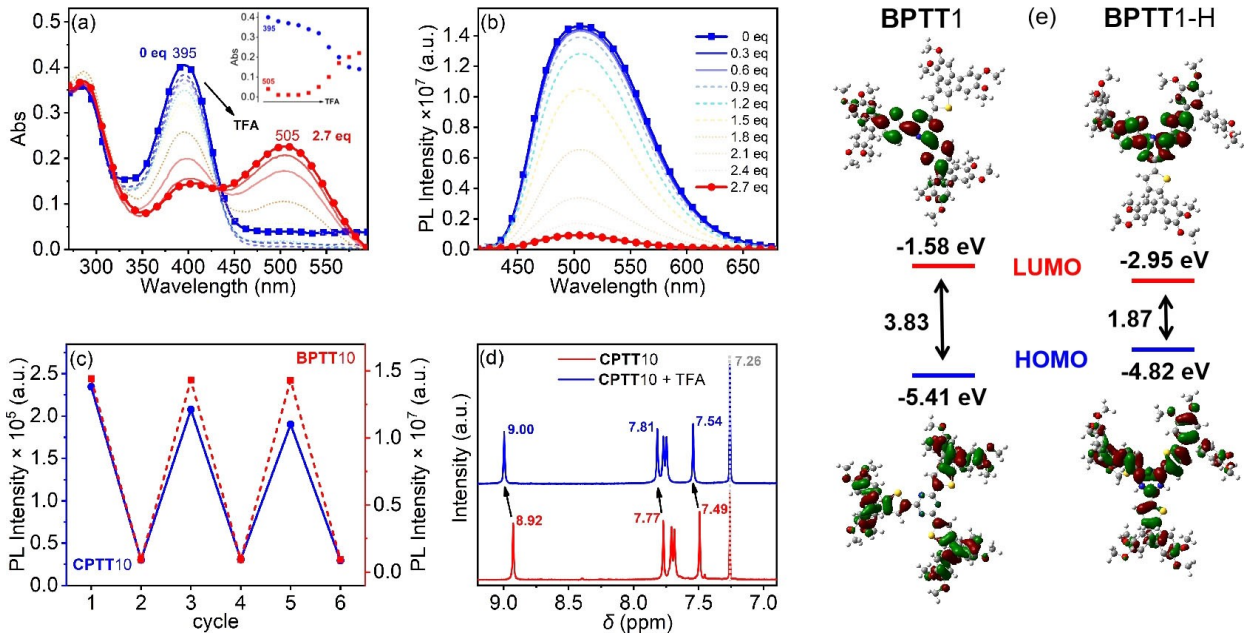

Figure 6. (a) and (b): UV absorption and photoluminescence spectra of **BPTT**10 in $CHCl_3$ with addition of TFA; (c): TFA and TEA stimuli-responsive fluorescence of **BPTT**10 and **CPTT**10; (d): ^{1}H NMR spectrum of **CPTT**10 with TFA treatment; (e): frontier molecular orbital electron cloud distribution and band gap of **BPTT**1 and protonated **BPTT**1-**H**.

and **CPTT**10 were not damaged, only a reversible protonation and deprotonation of the triazine core occurred.

In order to study the essence of their acidochromism, the ^{1}H NMR spectra (Figure 6d) of **CPTT**10 was used for protonation/deprotonation observation. It was found that all the Ar**H** protons experienced various degrees of low-field shift after the addition of TFA. The protonation of the triazine core by TFA reduces the π-electron density and weakens the shielding effect on the **ArH**, demonstrating that the acidochromism in the absorption and emission quenching are rooted in the protonation reaction between TFA and the triazine core.[8,45] For further evidence to support the mechanism of fluorescence changes in the process of acidochromism, DFT calculations were conducted on **BPTT**1 and its protonated product **BPTT**1-H at the theoretical level of Gaussian 09 W B3LYP/6-31G* (Figure 6e). In **BPTT**1, the electron distribution is mainly on the electron-donating biphenyl and thiophene parts in the HOMO, while in the LUMO, the electron distribution is located on the strong electron-withdrawing triazine core. This is consistent with an intramolecular charge transfer (ICT) phenomenon with a band gap of 3.83 eV by photo-excitation. After protonation, the triazine core becomes more electron-deficient, and the enhanced electron-withdrawing ability leads to a more concentrated distribution of the LUMO orbital electron cloud on the triazine. The energy gap is reduced to 1.87 eV, which explains the huge red-shift of the absorption and acidochromism. In addition, the protonated **BPTT**1-H exhibits a higher distorted conformation (Figure S17). The twisted intramolecular charge transfer (TICT) results in the fluorescence quenching. In summary, all the results show that **CPTT**10 and **BPTT**10 have application potential in information processing and acid-base sensing.

More interestingly, this acidochromism does not only exist in the solution of **BPTT**10 and **CPTT**10, but also in the aggregation states of powder and thin film. Based on this acidochromism, the potential for data rewriting paper and fluorescence printing technique for information processing was investigated (Figure 7). A chloroform solution of **BPTT**10 was uniformly dropped on a filter paper. After evaporation of solvent, a light-yellow colored paper was obtained, which was bright green under a 365 nm UV lamp. A leaf pattern was printed on the paper by TFA fumigation. The dark leaf shape on the paper displays higher contrast under UV light. After fumigating the paper with TEA, the patterns under daylight and UV light disappear. With the help of mask and TFA fuming, a new pattern can be printed on the paper or erased by the TEA fumigation. This simple process for engraving and data replication of a fluorescent pattern can be repeated multiple times with a remarkable reproducibility. This technique was implemented with **CPTT**10. However, the strong π–π stacking of **CPTT**10 in the solid state produced aggregation fluorescence quenching, resulting in non-obvious phenomena compared with **BPTT**10 (Figure 7).

Metal Ion Recognition

Metal ion recognition materials are particular stimulus-responsive materials, and are widely used in fluorescence sensors for heavy metal detection because of the ability to specifically recognize metal ion.[46,47] The fluorescence changes caused by metal ions are generally attributed to coordination or heavy atom effects. Given the strong coordination ability of N and S atoms in **BPTT***n* and **CPTT***n*, we employed **BPTT**10 and **CPTT**10

© 2024 The Authors. Chemistry - A European Journal published by Wiley-VCH GmbH

15213765, 0, Downloaded from https://chemistry-europe.onlinelibrary.wiley.com/doi/10.1002/chem.202400296 by Cochrane France, Wiley Online Library on [03/05/2024]. See the Terms and Conditions (https://onlinelibrary.wiley.com/terms-and-conditions) on Wiley Online Library for rules of use; OA articles are governed by the applicable Creative Commons License

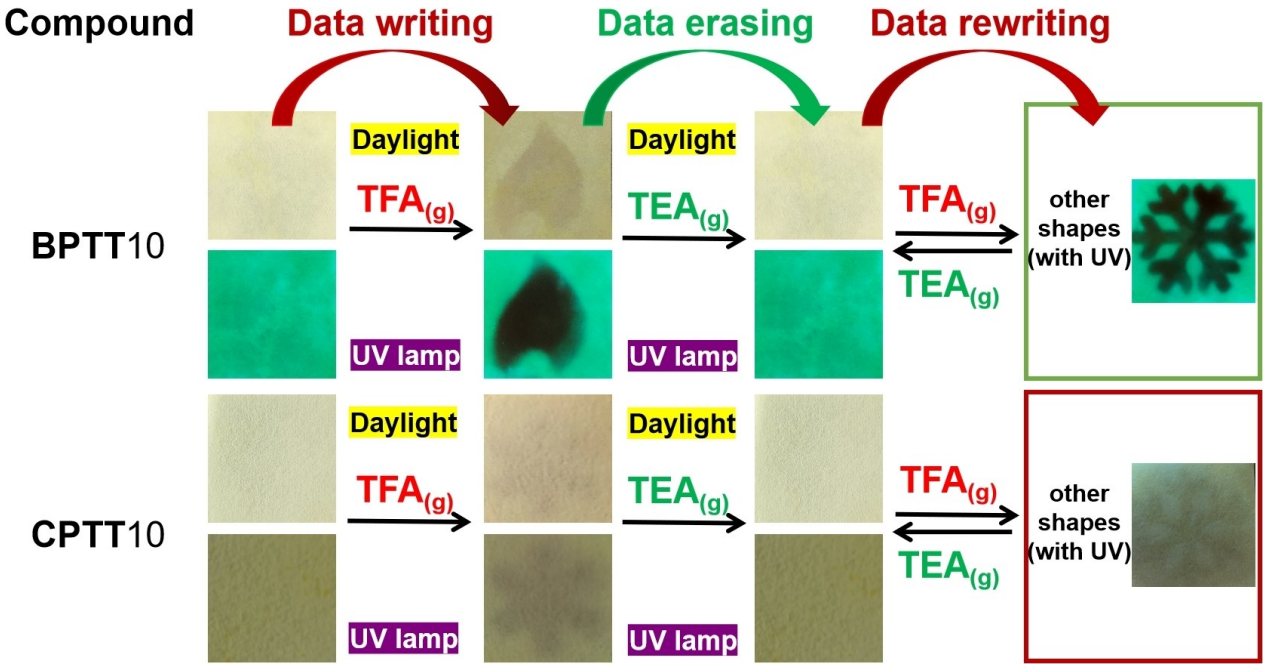

Figure 7. Acid-base stimuli-responsive fluorescent emission of the star-shape triazine-cored **BPTT**10 and **CPTT**10. TFA, CF_3COOH; TEA, Et_3N.

to investigate their properties in metal ion recognition, and the results are shown in Figure 8. When 4.0 equivalents of nine aqueous solutions of common metal salt (1 eq. = 10^{-5} mol/L) were added to **BPTT**10 and **CPTT**10 in THF, it was found that the addition of Fe^{3+} resulted in a significant attenuation of the fluorescence, while no change in fluorescence was observed when other metal ions were added. In order to eliminate the interference of anions, we tested the fluorescence spectra of **BPTT**10 and **CPTT**10 in THF with sodium salts (4.0 eq.) containing different anions, and no fluorescence quenching was observed. These observations reveal that **BPTT**10 and **CPTT**10 are capable of specific Fe^{3+} recognition. This specific recognition may be attributed to the stronger interaction between Fe^{3+} as a hard acid and triazine as a hard base. In addition, when Fe^{3+} was added to a solution containing metal ions (non-iron ions), the fluorescence was also quenched, which proves that **BPTT**10 (**CPTT**10) also have an anti-interference ability for this specific recognition ability of Fe^{3+}. By successively adding $FeCl_3$ solution to **BPTT**10 in THF, it was found that the fluorescence intensity gradually weakened, and the fluorescence hardly changed after adding >3.0 eq. It was speculated that Fe^{3+} and **BPTT**10 (**CPTT**10) form a complex with a binding ratio of 3:1. Ethylenediaminetetraacetic acid (EDTA) is a strong chelating agent, which can form a stable chelates with Fe^{3+}. In order to confirm the coordination of Fe^{3+} with **BPTT**10, EDTA was added to the solution after fluorescence quenching, and it was found that the fluorescence emission was gradually recovered, due to stronger coordination ability of Fe^{3+} with EDTA than with **BPTT**10. Therefore, it can be inferred that the addition of Fe^{3+} did not damage the chemical structure of **BPTT**10 (**CPTT**10). In addition, ^{1}H NMR spectroscopic experiments of **BPTT**10 in $CDCl_3$ before and after adding Fe^{3+} were performed (Figure 8f). When $FeCl_3$ was added to **BPTT**10, a broad peak was formed, caused by the paramagnetism of Fe^{3+}. However, it was not difficult to see that the two sets of hydrogen chemical shifts on the thiophene unit have different degrees of high field shifts, and the positions of the rest of the hydrogen remained virtually unchanged. This may be due to the coordination of Fe^{3+} with the N and S atoms in the **BPTT**10 to form a chelate, and the shielding effect of the large electron cloud density of Fe^{3+} and Cl^- causes the adjacent H signals to shift to high field. Furthermore, Fe^{3+} may also promote molecular aggregation through cation-π interactions, which may also lead to high-field displacement of the proton signals. A dynamic light scattering experiment on the particle size distribution in solutions with different ions showed that the particle size of the Fe^{3+} solution was smaller, which proved that Fe^{3+} was more likely to cause molecular aggregation in solution (Figure S31).

In order to further explore the mechanism of fluorescence quenching caused by the Fe^{3+}, the optimized conformation and frontier molecular orbital electron cloud distribution of **BPTT**1-Fe were calculated by DFT at the theoretical level of Gaussian 09W B3LYP/6-31G* (Figure S17). In the HOMO orbital of **BPTT**1-Fe, the electron cloud coordinated by Fe^{3+} is mainly distributed on the two biphenyl units, and the electron cloud density resides on the thiophene unit as the electron donor π bridge is weakened. Because the triazine unit and Fe^{3+} are strong electron-withdrawing units, in the LUMO orbital, electrons are transferred from biphenyl to triazine and Fe^{3+}. Fe^{3+}, with a d^5 electron configuration and a forbidden transition, is allowed to produce greater absorption when it obtains electrons. However, the Jahn-Teller effect caused by the asymmetric distribution of electrons in the degenerate orbit when d^5 is filled by electrons,

© 2024 The Authors. Chemistry - A European Journal published by Wiley-VCH GmbH

15213765, 0, Downloaded from https://chemistry-europe.onlinelibrary.wiley.com/doi/10.1002/chem.202400296 by Cochrane France, Wiley Online Library on [03/05/2024]. See the Terms and Conditions (https://onlinelibrary.wiley.com/terms-and-conditions) on Wiley Online Library for rules of use; OA articles are governed by the applicable Creative Commons License

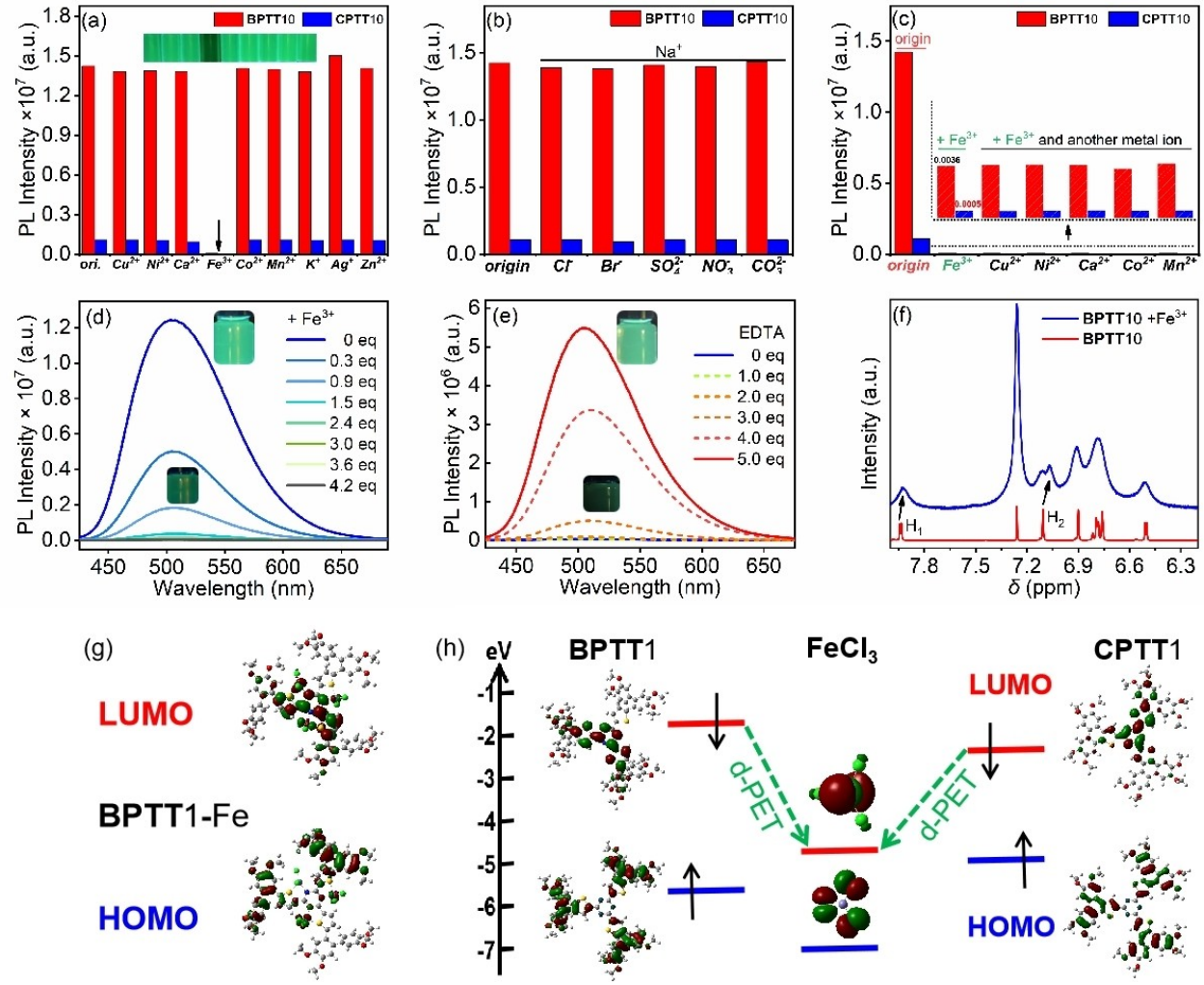

Figure 8. Metal ion selective fluorescence quenching. (a): Photoluminescent intensity of **BPTT**10 and **CPTT**10 treated with various metal ions, insert shows fluorescent photos of **BPTT**10 with ion; (b): Photoluminescent intensity of **BPTT**10 and **CPTT**10 with sodium salts of different anions; (c): Photoluminescent intensity of **BPTT**10 and **CPTT**10 with only Fe^{3+} and both Fe^{3+} and another metal ion; (d): Photoluminescent spectra of **BPTT**10 in THF quenched by $FeCl_3$; (e): Fluorescence recovery by addition of EDTA; (f): ^1H NMR spectra of **BPTT**10 before and after $FeCl_3$ addition; (g): HOMO/LUMO of **BPTT**1-Fe; (h): Photoinduced electron transfer (PET) process between **BPTT**1/**CPTT**1 and $FeCl_3$.

will distort the molecular geometry and weaken the molecular symmetry, which is essentially not conducive to the ICT effect. In addition, the fluorescence changes caused by metal ion coordination are often accompanied by a photoinduced electron transfer (PET) process. To explore whether the fluorescence quenching process is related to the PET process, we continued to calculate the frontier molecular orbitals of the guest molecule ($FeCl_3$). The results show that the LUMO orbital energy level (5.02 eV) of $FeCl_3$ is located between the HOMO and LUMO orbitals of **BPTT**1 (**CPTT**1), which means that the excited state electrons of **BPTT**1 (**CPTT**1) in the LUMO can be directly transferred to the empty orbital of the guest molecule ($FeCl_3$) and cannot be directly returned to the ground state to cause fluorescence quenching. This is a typical d-PET process. Therefore, the main mechanism of the fluorescence changes of **BPTT**10 (**CPTT**10) on the specific recognition of Fe^{3+} is the combination of the weakening of the ICT effect and the appearance of the d-PET process.

Conclusions

In this paper, we report two series of star-shaped, thiophene-containing triazine multifunctional materials, **BPTT***n* and **CPTT***n*, which are prepared by a combination of Suzuki-Mayaura coupling and Scholl oxidative dehydrogenation cyclization reaction. In THF, **BPTT***n* and **CPTT***n* exhibit green and yellow photoluminescence, respectively, which still exists in the thin film state. **BPTT***n* and **CPTT***n* exhibit different degrees of solvatochromic behavior due to the influence of intramolecular charge transfer. The fitting of the Lippert-Magata equation showed that **BPTT***n* is more sensitive to solvent polarity, and the polarity change shows a linear relationship with Stokes shift (of $R^2 = 0.99$), showing that the latter has the potential to be developed as a solvatochromic fluorescent probe. Due to the easy protonation of triazine core nuclei, **BPTT***n* and **CPTT***n* show also obvious acidochromic behavior. DFT calculations demonstrate that the enhancement of the electron-withdraw-

© 2024 The Authors. Chemistry - A European Journal published by Wiley-VCH GmbH

15213765, 0, Downloaded from https://chemistry-europe.onlinelibrary.wiley.com/doi/10.1002/chem.202400296 by Cochrane France, Wiley Online Library on [03/05/2024]. See the Terms and Conditions (https://onlinelibrary.wiley.com/terms-and-conditions) on Wiley Online Library for rules of use; OA articles are governed by the applicable Creative Commons License

ing ability of the triazine unit after TFA protonation leads to the decrease of the band gap and to the change of the electron cloud distribution, which is the fundamental reason for the red shift of the wavelength and the fluorescence quenching. Based on their acidochromic behavior, fluorescence anti-counterfeiting can be designed. Among the common metal ions, **BPTT***n* and **CPTT***n* can specifically recognize Fe^{3+}, and the DFT computing shows that the photoinduced electron transfer process is the key to fluorescence quenching. In terms of liquid crystal properties, **BPTT***n* failed to self-assemble into a liquid crystal mesophase due to molecular distortion and excessive flexibility. By contrast, **CPTT***n* can self-assemble to form a Col_{rec} mesophase during the temperature change process and show a tendency to reduce the mesophase range with the increase of the flexible chain-length. As the triazine unit can interact with protons, the formation of intermolecular hydrogen bonds between oleic acid and **CPTT**10 can easily be formed, allowing to modulate the liquid crystal properties from Col_{rec} to Col_{hex} mesophase and substantially to reduce the clearing point of **CPTT**10. In addition, this self-assembly ability was also reflected in the gelation of **CPTT***n* whose self-assembly ability enables it to form organogels in different solvents. The critical gel concentration of **CPTT**10 in cyclohexane and hexane is as low as 3.0 mg/mL. It can be seen that these star-shaped, triazine-thiophene derivatives not only have potential applications in fluorescence sensing, information processing, but also have development space for liquid crystal semiconductors and organic gelators.

Supporting Information

Experimental methods, materials and instrumentation, synthetic details, and characterization, ^{1}H and ^{13}C NMR (Figures S1–7, S20), HRMS (Figures S8–12), EA, TGA (Figure S13, Table S1), DSC (Figure S14, Table S2), POM (Figures S15), DFT (Figures S16–17), S/WAXS (Figures S18–19, Table S3), UV absorption and photoluminescence (Figures S21–24, Table S4), DLS (Figure S26), are given in the supporting information.

Acknowledgements

Z. C. Y. and D. W. J. contribute equally to this work. We thank the National Natural Science Foundation of China for funding (51773140). B. D. thanks the CNRS and the University of Strasbourg for constant support.

Conflict of Interests

The authors declare no conflict of interest.

Data Availability Statement

The data that support the findings of this study are available in the supplementary material of this article.

Keywords: Triazine · Discotic liquid crystal · Stimuli responsive luminescence · Metal ion recognition · Phenanthrothiophene

[1] a) H. Detert, M. Lehmann, H. Meier, *Materials* **2010**, *3*, 3218–3330; b) M. Lehmann, *Chem. Eur. J.* **2009**, *15*, 3638–3651.
[2] Y. Jiang, Y. Wang, J. Hua, J. Tang, B. Li, S. Qian, H. Tian, *Chem. Commun.* **2010**, *46*, 4689–4691.
[3] J. Mei, N. L. C. Leung, R. T. K. Kwok, J. W. Y. Lam, B. Z. Tang, *Chem. Rev.* **2015**, *115*, 11718–11940.
[4] Y. Sun, J. Zhang, H. Yu, C. Huang, J. Huang, *ACS Appl. Mater. Interfaces* **2022**, *14*, 6625–6637.
[5] D. Wagner, S. T. Hoffmann, U. Heinemeyer, I. Münster, A. Köhler, P. Strohriegl, *Chem. Mater.* **2013**, *25*, 3758–3765.
[6] T. Yasuda, T. Shimizu, F. Liu, G. Ungar, T. Kato, *J. Am. Chem. Soc.* **2011**, *133*, 13437–13444.
[7] a) T. Jarosz, M. Lapkowski, P. Ledwon, *Macromol. Rapid Commun.* **2014**, *35*, 1006–1032; b) A. L. Kanibolotsky, I. F. Perepichka, P. J. Skabara, *Chem. Soc. Rev.* **2010**, *39*, 2695–2728; c) A. L. Kanibolotsky, N. Laurand, M. D. Dawson, G. A. Turnbull, I. D. W. Samuel, P. J. Skabara, *Acc. Chem. Res.* **2019**, *52*, 1665–1674; d) H. M. Diab, A. M. Abdelmoniem, M. R. Shaaban, I. A. Abdelhamid, A. H. M. Elwahy, *RSC Adv.* **2019**, *9*, 16606–16682.
[8] a) C. Zeng, P. Hu, B. Wang, W. Fang, K. Zhao, B. Donnio, *Acta Chim. Sin.* **2023**, *81*, 469–479; b) N. R. Kumar, A. R. Agrawal, *ChemistryOpen* **2023**, *12*, e202200203; c) A. H. M. Elwahy, M. R. Shaaban, I. A. Abdelhamid, *Adv. Heterocycl. Chem.* **2023**, *140*, 233–301.
[9] a) A. Majeed Ganai, T. Khan Pathan, G. A. Hampannavar, C. Pawar, V. A. Obakachi, B. Kushwaha, N. Deshwar Kushwaha, R. Karpoormath, *ChemistrySelect* **2021**, *6*, 1616–1660; b) F. G. Zhang, Z. Chen, X. Tang, J.-A. Ma, *Chem. Rev.* **2021**, *121*, 14555–14593; c) D. Sun, C. Si, T. Wang, E. Zysman-Colmna, *Adv. Photonics Res.* **2022**, *3*, 2200203; d) V. Dávila Cerón, L. A. Illicachi, B. Insuasty, *Molecules* **2023**, *28*, 257.
[10] a) C.-H. Lee, T. Yamamoto, *Bull. Chem. Soc. Jpn.* **2002**, *75*, 615–618; b) C.-H. Lee, T. Yamamoto, *Tetrahedron Lett.* **2001**, *42*, 3993–3996; c) L. L. Lai, C. H. Lee, L. Y. Wang, K. L. Cheng, H. F. Hsu, *J. Org. Chem.* **2008**, *73*, 485–490; d) S. Kotha, D. Kashinath, S. Kumar, *Tetrahedron Lett.* **2008**, *49*, 5419–5423.
[11] H. Lee, D. Kim, H.-K. Lee, W. Qiu, N.-K. Oh, W.-C. Zin, K. Kim, *Tetrahedron Lett.* **2004**, *45*, 1019–1022.
[12] P. Bhagavath, R. Shetty, D. Sunil, *Critical Rev. Sol. State Mater. Sci.* **2020**, *45*, 378–409.
[13] a) F. N. da Silva, H. M. Luciano, C. H. Stadtlober, G. Farias, F. Durola, J. Eccher, I. H. Bechtold, H. Bock, H. Gallardo, A. A. Vieira, *Chem. Eur. J.* **2023**, *29*, e202301319; b) F. N. da Silva, H. Marchi Luciano, C. H. Stadtlober, G. Farias, F. Durola, J. Eccher, I. H. Bechtold, H. Bock, H. Gallardo, A. A. Vieira, *Chem. Eur. J.* **2023**, *29*, e202203604.
[14] a) S. Laschat, A. Baro, N. Steinke, F. Giesselmann, C. Hägele, G. Scalia, R. Judele, E. Kapatsina, S. Sauer, A. Schreivogel, M. Tosoni, *Angew. Chem. Int. Ed.* **2007**, *46*, 4832–4887; *Angew. Chem.* **2007**, *119*, 4916–4973; b) T. Wöhrle, I. Wurzbach, J. Kirres, A. Kostidou, N. Kapernaum, J. Litterscheidt, J. C. Haenle, P. Staffeld, A. Baro, F. Giesselmann, S. Laschat, *Chem. Rev.* **2016**, *116*, 1139–1241; c) T. Kato, J. Uchida, T. Ichikawa, T. Sakamoto, *Angew. Chem. Int. Ed.* **2018**, *57*, 4355–4371; *Angew. Chem.* **2018**, *130*, 4438–4455.
[15] R. Termine, A. Golemme, *Int. J. Mol. Sci.* **2021**, *22*, 877.
[16] a) X. Feng, V. Marcon, W. Pisula, M. R. Hansen, J. Kirkpatrick, F. Grozema, D. Andrienko, K. Kremer, K. Müllen, *Nat. Mater.* **2009**, *8*, 421–426; b) X. Crispin, J. Cornil, R. Friedlein, K. Kamiya Okudaira, V. Lemaur, A. Crispin, G. Kestemont, M. Lehmann, M. Fahlman, R. Lazzaroni, Y. Geerts, G. Wendin, N. Ueno, J.-L. Brédas, W. R. Salaneck, *J. Am. Chem. Soc.* **2004**, *126*, 11889–11899.
[17] a) K. Q. Zhao, C. Chen, H. Monobe, P. Hu, B. Q. Wang, Y. Shimizu, *Chem. Commun.* **2011**, *47*, 6290–6292; b) K.-Q. Zhao, L.-L. An, X.-B. Zhang, W.-H. Yu, P. Hu, B.-Q. Wang, J. Xu, Q.-D. Zeng, H. Monobe, Y. Shimizu, B. Heinrich, B. Donnio, *Chem. Eur. J.* **2015**, *21*, 10379–10390.

© 2024 The Authors. Chemistry - A European Journal published by Wiley-VCH GmbH

15213765, 0, Downloaded from https://chemistry-europe.onlinelibrary.wiley.com/doi/10.1002/chem.202400296 by Cochrane France, Wiley Online Library on [03/05/2024]. See the Terms and Conditions (https://onlinelibrary.wiley.com/terms-and-conditions) on Wiley Online Library for rules of use; OA articles are governed by the applicable Creative Commons License

[18] a) M. O'Neill, S. M. Kelly, *Adv. Mater.* **2011**, *23*, 566–584; b) M. O'Neill, S. M. Kelly, *Adv. Mater.* **2003**, *15*, 1135–1146; c) W. Pisula, X. Feng, K. Müllen, *Adv. Mater.* **2010**, *22*, 3634–3649.
[19] a) T. Reppe, C. Dressel, S. Poppe, A. Eremin, C. Tschierske, *Adv. Opt. Mater.* **2020**, *9*, 2001572; b) T. Yasuda, H. Ooi, J. Morita, Y. Akama, K. Minoura, M. Funahashi, T. Shimomura, T. Kato, *Adv. Funct. Mater.* **2009**, *19*, 411–419; c) J. M. Wolska, N. Topnani, E. Gorecka, J. Mieczkowski, D. Pociecha, *ChemPhysChem* **2016**, *17*, 2686–2690; d) R. Zuo, S. Wang, Y. Pang, Y. Xiao, Z. Jiang, *Dyes Pigm.* **2021**, *188*, 109153; e) H. Zhao, X. Cheng, *Int. J. Mol. Sci.* **2023**, *24*, 9337; f) F. Lincker, P. Bourgun, P. Masson, P. Didier, L. Guidoni, J. Y. Bigot, J. F. Nicoud, B. Donnio, D. Guillon, *Org. Lett.* **2005**, *7*, 1505–1508; g) N. H. Sultana, S. M. Kelly, B. Mansoor, M. O'Neill, *Liq. Cryst.* **2007**, *34*, 1307–1316; h) Y. Liang, X. Liu, Y. Pu, R. Zhang, L. Zhou, Y. Xiao, *J. Lumin.* **2023**, *262*, 119977; i) Y. Xiao, X. Liu, N. Li, Z. Zheng, *J. Mol. Liq.* **2022**, *364*, 120029.
[20] a) A. C. Grimsdale, K. Müllen, *Angew. Chem. Int. Ed.* **2005**, *44*, 5592–5629; *Angew. Chem.* **2005**, *117*, 5732–5772; b) X. Feng, W. Pisula, K. Müllen, *Pure Appl. Chem.* **2009**, *81*, 2203–2224; c) A. N. Cammidge, *Phil. Trans. R. Soc. A* **2006**, *364*, 2697–2708; d) M. Stępień, E. Gońka, M. Żyła, N. Sprutta, *Chem. Rev.* **2017**, *117*, 3479–3716.
[21] a) T. Ma, H. Wang, K. Zhao, B. Wang, P. Hu, H. Monobe, B. Heinrich, B. Donnio, *ChemPlusChem.* **2019**, *84*, 1439–1448; b) W. Deng, S. Liu, H. Lin, K. Zhao, X. Bai, K. Zhao, P. Hu, B. Wang, H. Monobe, B. Donnio, *New J. Chem.* **2022**, *46*, 7936–7949; c) T. Ma, Y. Zhong, H. Wang, K. Zhao, B. Wang, P. Hu, H. Monobe, B. Donnio, *Chem. Asian J.* **2021**, *16*, 1106–1117; d) K. Zhao, J. Du, H. Wang, K. Zhao, P. Hu, B. Wang, H. Monobe, B. Heinrich, B. Donnio, *Chem. Asian J.* **2019**, *14*, 462–470; e) C. X. Liu, H. Wang, J. Q. Du, K. Q. Zhao, P. Hu, B. Q. Wang, H. Monobe, B. Heinrich, B. Donnio, *J. Mater. Chem. C* **2018**, *6*, 4471–4778.
[22] a) E. Beltran, B. Robles-Hernandez, N. Sebastian, J. Luis Serrano, R. Gimenez, T. Sierra, *RSC Adv.* **2014**, *4*, 23554–23561; b) M. Masuda, M. Kohri, K. Kishikawa, *Liq. Cryst.* **2021**, *48*, 295–306; c) M. Martinez-Abadia, S. Varghese, J. Gierschner, R. Giménez, M. Blanca-Ros, *J. Mater. Chem. C* **2022**, *10*, 12012–12021.
[23] L. X. Guo, Y. B. Xing, M. Wang, Y. Sun, X. Q, Zhang, B. P. Lin, H. Yang, *J. Mater. Chem. C* **2019**, *7*, 4828–4837.
[24] a) B. Mu, Y. Zhao, X. Li, X. Quan, W. Tian, *ACS Appl. Mater. Interfaces* **2020**, *12*, 9637–9645; b) B. Mu, T. Ma, Z. Zhang, X. Hao, L. Wang, J. Wang, H. Yan, W. Tian, *Chem. Eur. J.* **2023**, *29*, e202300320.
[25] a) K. Noll, M. Lambov, D. P. Singh, M. Lehmann, *Chem. Eur. J.* **2023**, *29*, e202303375; b) M. Lambov, P. Maier, M. Jasiński, J. Szczytko, P. Kaszyński, M. Lehmann, *J. Mater. Chem. C* **2022**, *10*, 8728–8739; c) M. Lehmann, M. Dechant, M. Lambov, T. Ghosh, *Acc. Chem. Res.* **2019**, *52*, 1653–1664; d) M. Lambov, N. Hensiek, A. C. Pöppler, M. Lehmann, *ChemPlusChem* **2020**, *85*, 2219–2229.
[26] a) B. N. Veerabhadraswamy, H. K. Dambal, D. S. Shankar Rao, C. V. Yelamaggad, *ChemPhysChem* **2016**, *17*, 2225–2237; b) F. A. Olate, J. A. Ulloa, J. M. Vergara, S. A. Sánchez, J. Barberá, M. L. Parra, *Liq. Cryst.* **2016**, *43*, 811–827; c) B. Pradhan, S. K. Pathak, R. K. Gupta, M. Gupta, S. K. Pal, A. A. Sudhakar, *J. Mater. Chem. C* **2016**, *4*, 6117–6130.
[27] a) N. Tober, T. Rieth, M. Lehmann, H. Detert, *Chem. Eur. J.* **2019**, *25*, 15295–15304; b) A. Martínez-Bueno, R. Vidal, J. Ortega, J. Etxebarria, C. L. Folcia, R. Giménez, T. Sierra, *Mat. Today Chem.* **2023**, *29*, 101394.
[28] a) T. Wöhrle, H. Taing, C. Schilling, S. H. Eichhorn, S. Laschat, *Liq. Cryst.* **2019**, *46*, 1973–1984; b) M. Lehmann, M. Dechant, *Liq. Cryst.* **2019**, *46*, 1214–1222; c) M. Lehmann, M. Dechant, L. Gerbig, M. Baumann, *Liq. Cryst.* **2019**, *46*, 1985–1994; d) S. Roth, M. Lehmann, *Liq. Cryst.* **2017**, *44*, 1830–1851.
[29] H. Taing, J. G. Rothera, J. F. Binder, C. L. B. Macdonald, S. H. Eichhorn, *Liq. Cryst.* **2018**, *45*, 1147–1154.
[30] F. Yang, J. Xie, H. Guo, B. Xu, C. Li, *Liq. Cryst.* **2012**, *39*, 1368–1374.
[31] Y. Bai, L. Chen, P. Hu, K. Luo, W. Yu, H. Ni, K. Zhao, B. Wang, *Liq. Cryst.* **2015**, *42*, 1591–1600.
[32] a) B. Feringan, P. Romero, J. L. Serrano, R. Gimenez, T. Sierra, *Chem. Eur. J.* **2015**, *21*, 8859–8866; b) B. Feringan, P. Romero, J. L. Serrano, C. L. Folcia, J. Etxebarria, J. Ortega, R. Termine, A. Golemme, R. Giménez, T. Sierra, *J. Am. Chem. Soc.* **2016**, *138*, 12511–12518.
[33] B. Feringán, R. Termine, A. Golemme, J. M. Granadino-Roldán, A. Navarro, R. Giménez, T. Sierra, *J. Mater. Chem. C.* **2021**, *9*, 1972–1982.
[34] X. Cheng, J. Jin, Q. Li, X. Dong, *Chin. J. Chem.* **2010**, *28*, 1957–1962.
[35] a) Y. Li, A. Concellon, C. J. Lin, N. A. Romero, S. Lin, T. M. Swager, *Chem. Sci.* **2020**, *11*, 4695–4701; b) H. Lin, K. Zhao, M. Jing, X. Long, K. Zhao, P. Hu, B. Wang, P. Lei, Q. Zeng, B. Donnio, *J. Mater. Chem. C.* **2022**, *10*, 14453–14470.
[36] J. Hang, H. Lin, K. Zhao, P. Hu, B. Wang, H. Monobe, C. Zhu, B. Donnio, *Eur. J. Org. Chem.* **2021**, *13*, 1989–2002.
[37] Q. Zeng, S. Liu, H. Lin, K. Zhao, X. Bai, K. Zhao, P. Hu, B. Wang, B. Donnio, *Molecules* **2023**, *28*, 1721.
[38] J. Dai, K. Zhao, B. Wang, P. Hu, B. Heinrich, B. Donnio, *J. Mater. Chem. C.* **2020**, *8*, 4215–4225.
[39] X. Zhu, X. Bai, H. Wang, P. Hu, B. Wang, K. Zhao, *Acta Chim. Sin.* **2021**, *79*, 1486–1493.
[40] a) C. M. Paleos, D. Tsiourvas, *Angew. Chem. Int. Ed.* **1995**, *34*, 1696–1911; *Angew. Chem.* **1995**, *107*, 1839–1855; b) C. M. Paleos, D. Tsiourvas, *Liq. Cryst.* **2001**, *28*, 1127–1161; c) T. Kato, N. Mizoshita, K. Kishimoto, *Angew. Chem. Int. Ed.* **2006**, *45*, 38–68; *Angew. Chem.* **2006**, *118*, 44–74; d) C. Tschierske, *Angew. Chem. Int. Ed.* **2013**, *52*, 8828–8878; *Angew. Chem.* **2013**, *125*, 8992–9047; e) B. M. Rosen, C. J. Wilson, D. A. Wilson, M. Peterca, M. R. Imam, V. Percec, *Chem. Rev.* **2009**, *109*, 6275–6540; f) T. Kato, *Struct. Bonding (Berlin)* **2000**, *96*, 95–146.
[41] B. Donnio, B. Heinrich, H. Allouchi, J. Kain, S. Dele, D. Guillon, D. W. Bruce, *J. Am. Chem. Soc.* **2004**, *126*, 15258–15268.
[42] a) S. S. Babu, V. K. Praveen, A. Ajayaghosh, *Chem. Rev.* **2014**, *114*, 1973–2129; b) M. Liu, G. Ouyang, D. Niu, Y. Sang, *Org. Chem. Front.* **2018**, *5*, 2885–2900; c) T. Kato, Y. Hirai, S. Nakaso, M. Moriyama, *Chem. Soc. Rev.* **2007**, *36*, 1857–1867.
[43] M.-M. Zhou, J. He, H.-M. Pan, Q. Zeng, H. Lin, K.-Q. Zhao, P. Hu, B.-Q. Wang, B. Donnio, *Chem. Eur. J.* **2023**, *29*, e202301829.
[44] a) S. J. D. Lugger, S. J. A. Houben, Y. Foelen, M. G. Debije, A. P. H. J. Schenning, D. J. Mulder, *Chem. Rev.* **2022**, *122*, 4946–4975; b) Y. Ni, X. Li, J. Hu, S. Huang, H. Yu, *Chem. Mater.* **2019**, *31*, 3388–3394; c) T. Kato, J. Uchida, T. Ichikawa, B. Soberats, *Polym. J.* **2018**, *50*, 149–166; d) E. Bukusoglu, M. Bedolla Pantoja, P. C. Mushenheim, X. Wang, N. L. Abbott, *Annu. Rev. Chem. Biomol. Eng.* **2016**, *7*, 163–96.
[45] M. Guerrini, E. D. Aznar, C. Cocchi, *J. Phys. Chem. C* **2020**, *124*, 27801–27810.
[46] S. K. Sahoo, D. Sharma, R. K. Bera, G. Crisponic, J. F. Callan, *Chem. Soc. Rev.* **2012**, *41*, 7195–7227.
[47] K. P. Carter, A. M. Young, A. E. Palmer, *Chem. Rev.* **2014**, *114*, 4564–4601.

Manuscript received: January 23, 2024
Accepted manuscript online: March 1, 2024
Version of record online: ■■, ■■

© 2024 The Authors. Chemistry - A European Journal published by Wiley-VCH GmbH

15213765, 0, Downloaded from https://chemistry-europe.onlinelibrary.wiley.com/doi/10.1002/chem.202400296 by Cochrane France, Wiley Online Library on [03/05/2024]. See the Terms and Conditions (https://onlinelibrary.wiley.com/terms-and-conditions) on Wiley Online Library for rules of use; OA articles are governed by the applicable Creative Commons License

RESEARCH ARTICLE

Triazine-based mesogens with three pending discoid arms have been shown to self-organize into rectangular columnar mesophases and form gels in various solvents. The solvatochromic-, acidochromic- and metal recognition-response photoluminescence of these mesogens offer applications in stimuli-responsive fluorescence anti-counterfeiting and as selective metal-ion recognition.

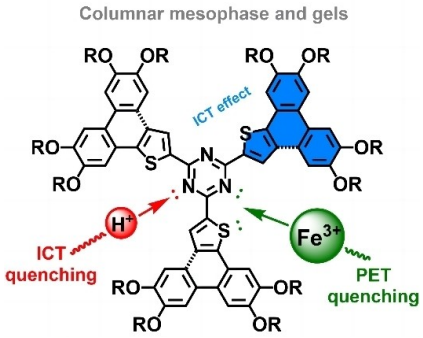

C.-Y. Zeng, W.-J. Deng, Prof. K.-Q. Zhao, Prof. C. Redshaw, Dr. B. Donnio**

15213765, 0, Downloaded from https://chemistry-europe.onlinelibrary.wiley.com/doi/10.1002/chem.202400296 by Cochrane France, Wiley Online Library on [03/05/2024]. See the Terms and Conditions (https://onlinelibrary.wiley.com/terms-and-conditions) on Wiley Online Library for rules of use; OA articles are governed by the applicable Creative Commons License